



Contents lists available at ScienceDirect



# Applied Catalysis A: General

journal homepage: [www.elsevier.com/locate/apcata](http://www.elsevier.com/locate/apcata)

## Hydrogen from steam reforming of ethanol over cobalt nanoparticles: Effect of boron impurities

Paola Riani<sup>a</sup>, Gabriella Garbarino<sup>b</sup>, A. Infantes-Molina<sup>c</sup>, Enrique Rodríguez-Castellón<sup>c,\*</sup>, Fabio Canepa<sup>a</sup>, Guido Busca<sup>b,\*\*</sup>

<sup>a</sup> Università degli Studi di Genova, Dipartimento di Chimica e Chimica Industriale (DCCI), Via Dodecaneso 31, 16146 Genova, Italy

<sup>b</sup> Università degli Studi di Genova, Dipartimento di Ingegneria Civile, Chimica e Ambientale (DICCA), Piazzale Kennedy 1, 16129 Genova, Italy

<sup>c</sup> Departamento de Química Inorgánica, Cristalografía y Mineralogía, Facultad de Ciencias, Universidad de Málaga, Campus de Teatinos, 29071 Málaga, Spain

### ARTICLE INFO

#### Article history:

Received 19 July 2015

Received in revised form 5 October 2015

Accepted 7 October 2015

Available online xxx

#### Keywords:

Cobalt nanoparticles

Ethanol steam reforming

Hydrogen

Catalysts

Cobalt XPS

### ABSTRACT

Cobalt nanoparticles have been prepared by reduction of cobalt chloride by sodium borohydride. They are very active catalysts for ethanol steam reforming at moderate temperature. The best catalytic materials show full ethanol conversion and hydrogen yields of the order of 83% and stable activity for 8 h when tested at 773 K, GHSV 324,000 h<sup>-1</sup> with diluted 1:6 ethanol:water feed in He 41.6%. The amount of coproduced methane is very low (yield <0.05%). Experiments performed at different space velocities provide evidence of the intermediate formation of acetaldehyde in the ethanol steam reforming path. The fresh Co nanopowders are amorphous and are actually contaminated mainly by Boron species and traces of Na, Cl and C. During reaction, Cobalt nanoparticles are transformed into cubic metallic Co crystallites. The surface properties of these materials are very sensitive to: (I) the separation procedure from the reaction medium at the end of the preparation step, and (II) the conditions of ageing and storage in the laboratory. An increasing time of ageing seems to favor the formation of borates species and the observed oxidation of metallic cobalt to cobalt oxides. These phenomena could be associated to the loss in the catalytic activity that results in a lower ethanol conversion, lower hydrogen yield and sometimes, higher selectivity to acetaldehyde.

© 2015 Published by Elsevier B.V.

## 1. Introduction

Bio-ethanol steam reforming is a possible way for producing renewable hydrogen and syngas [1–9]. In spite of the many studies undertaken recently on Ethanol Steam Reforming (ESR), no consensus was still obtained on the best conditions for performing ESR nor on the best catalyst formulation.

In the era of nanotechnology, catalysis by metal nanoparticles became a relevant field of investigation. In fact, a number of methods were developed allowing the preparation of well-characterized and shaped metal nanoparticles [10]. This allowed to test the effect of the size and shape of particles on catalytic activity. As for example, Alayouglu et al. [11] investigated monodisperse platinum nanoparticles with the shapes of octahedron, cube, truncated

octahedron, and sphere, and tested them in methyl-cyclopentane ring opening in the presence of hydrogen. These studies could also allow to compare the catalytic data with those arising from monocrystal data, thus attributing the catalysis on nanoparticles to the activity of the exposed faces or, alternatively, of corners and edges. On the other hand, metal nanoparticles are indeed very efficient catalysts for a number of organic reactions, as shown in the case of Pd nanocrystals [12]. However, the thermal stability of unsupported metal nanoparticles is generally weak, their applicability being usually limited to liquid phase reactions performed at low temperature; alternatively they may be essentially regarded as model catalysts, whose activity is limited to small time on stream experiments.

Cobalt is an active catalyst for a number of hydrogenation reactions. It has been used, mostly supported such as e.g., the Co/Al<sub>2</sub>O<sub>3</sub> or Co/SiO<sub>2</sub>-ZrO<sub>2</sub> catalysts, in the low-temperature Fischer Tropsch process [13], CoO/SiO<sub>2</sub> and CoO/SiO<sub>2</sub>-Al<sub>2</sub>O<sub>3</sub>, CoO/ZrO<sub>2</sub>-Kieselguhr catalysts for hydrogenation of oxoaldehydes and amination of alcohols and the reductive amination of aldehydes and ketones for the manufacture of ethylamines and propylamines [14–17].

\* Corresponding author. Fax: +34 952131870.

\*\* Corresponding author. Fax: +39 103536028.

E-mail addresses: [castellon@uma.es](mailto:castellon@uma.es) (E. Rodríguez-Castellón),

[Guido.Busca@unige.it](mailto:Guido.Busca@unige.it) (G. Busca).

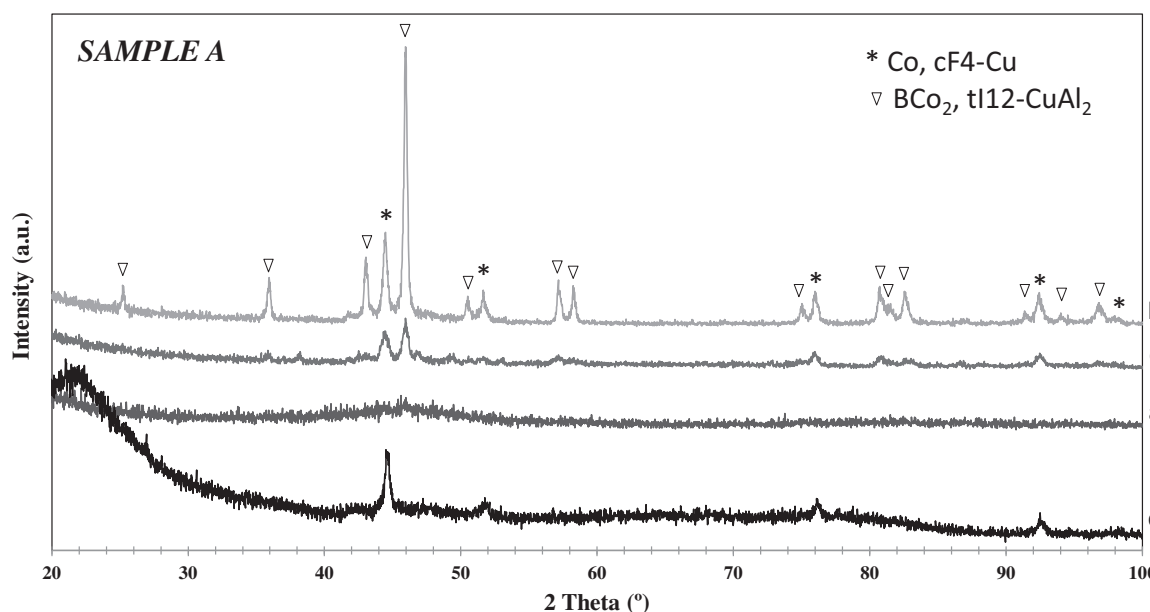


**Fig. 1.** XRD of catalyst A: fresh (a); after annealing at 773 K for 3 h in Ar (b); aged sample after annealing at 773 K for 3 h in Ar (c); exhaust sample after catalysis at 51,700 h<sup>-1</sup> (d).

Unsupported cobalt has been used in the past for Fischer Tropsch synthesis [18], while Raney-type “sponge” cobalt is commercially available for use in the hydrogenation of nitriles and nitro compounds to amines [19].

Unsupported cobalt catalysts produced by reducing Co oxide were found to be very active for ESR [20–22]. Recently, we found that unsupported cobalt nanoparticles (NPs), prepared by reducing Co chloride with NaBH<sub>4</sub>, may act as very good catalysts for ESR at least upon short time on stream experiments [23]. In particular, they allowed high hydrogen yield (over 85%) at moderate temperatures with low CO and CH<sub>4</sub> coproduction. XRD analysis did not show any crystalline phase in case of the fresh catalyst and the characteristic pattern of cubic metallic Co after its use. However, the fresh catalyst after annealing at the reaction temperature (773 K) also shows, besides the pattern of cubic Co metal, some reflections attributed to poorly crystallized cobalt boride Co<sub>2</sub>B, showing the presence of boron impurities and their strong interaction with cobalt. Indeed, the presence of impurities arising from the preparation procedure and from the precursor salts and their roles in modifying the catalyst behavior is a relevant point in the field of heterogeneous catalysis. With the preparation adopted, boron and sodium impurities arising from the reductant as well as chlorine arising from the cobalt source can be expected.

As a development of our previous work, we wanted to investigate whether the contamination of the nanoparticles could affect the catalytic activity of the resulting Co nanoparticles. In particular we will focus our attention on contamination by boron, the main contaminant residue of the reducing agent.

## 2. Experimental

### 2.1. Preparation of cobalt nanoparticles

Co-based nanoparticles were prepared using a reduction method in aqueous solution. In a typical synthesis procedure, a controlled excess of sodium borohydride is added as reducing agent to a 10<sup>-2</sup> M solution of CoCl<sub>2</sub>·6H<sub>2</sub>O maintained at room temperature under mechanical stirring and argon flux as described elsewhere [23,24]. The addition of the reductive agent is quickly followed by the appearance of a black precipitate. The reaction is then main-

tained for 15 min under the inert flux and stirring. The separation from the reaction medium and as well the washing procedure were carried out in different ways for the different samples prepared. Four samples, hereinafter denoted A–D, will be considered here. The different separation procedures will be described in the corresponding section. Depending on whether the sample has been tested and characterized few days after the preparation, several weeks or months after the preparation, or after catalytic runs, they will be denoted as “fresh”, “aged” or “exhaust”, respectively.

### 2.2. Characterization techniques

X-ray diffraction patterns on dried nanoparticles, annealed at 773 K for 3 h, and on the exhaust samples (after the ESR experiment) were carried out by using a vertical powder diffractometer X’Pert with Cu K $\alpha$  radiation ( $\lambda = 0.15406$  nm). The patterns were usually collected in the 25–100° 2 $\theta$  range with a step of 0.02° and a counting time for each step of at least 12 s. Powder patterns were indexed by comparing experimental results to the data reported in the Pearson’s Crystal Data database [25].

IR spectra were recorded with ThermoFisher Instrument using KBr pressed disks (1% wt/wt of sample, total weight 0.8080 g).

A scanning electron microscope ZEISS SUPRA 40 VP, with a field emission gun, was used to study the morphology of all the prepared catalysts (FE-SEM measurements). This instrument is equipped with a high sensitivity “InLens” secondary electrons detector and with an EDX microanalysis OXFORD “INCA Energie 450 × 3”. Samples for SEM analysis were suspended in ethanol and exposed to ultrasonic vibrations to decrease the aggregation. A drop of the resultant mixture was finally laid on a Lacey Carbon copper grid.

XPS measurements were performed using a Physical Electronics PHI 5700 spectrometer with non-monochromatic Mg K $\alpha$  radiation (300 W, 15 kV, and 1253.6 eV) and Al K $\alpha$  radiation (300 W, 15 kV, and 1456.6 eV) with a multi-channel detector. Spectra of fresh, aged or exhausted samples were recorded in the constant pass energy mode at 29.35 eV, using a 720  $\mu$ m diameter analysis area. Charge referencing was measured against adventitious carbon (C 1s at 284.8 eV). A PHIACCESS ESCA-V6.0 F software package was used for acquisition and data analysis. A Shirley-type background was subtracted from the signals. Recorded spectra were always fitted

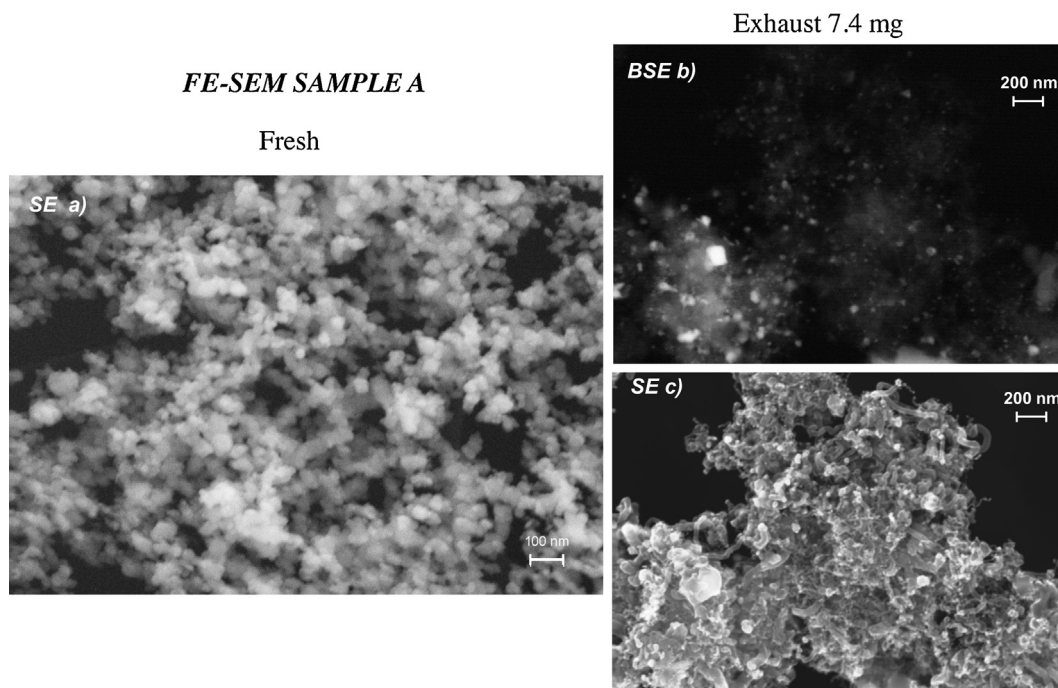


**Fig. 2.** FE-SEM micrographs of A sample: fresh (a); exhaust after catalytic experiment, BSE micrograph (b) and SE micrograph (c).

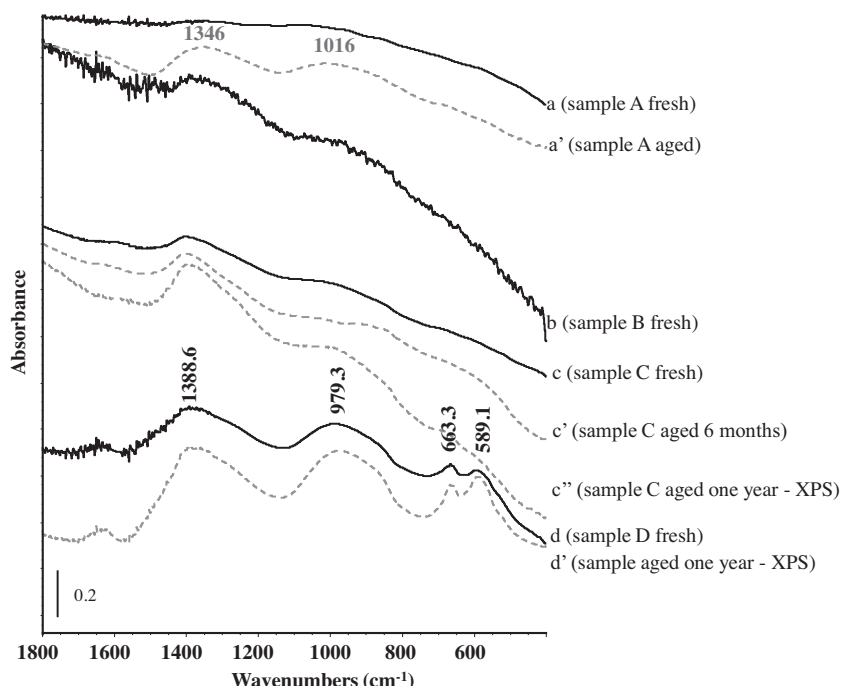


**Fig. 3.** IR spectra of the investigated catalysts: sample A fresh (a) and aged (a'); sample B fresh (b); sample C fresh (c), aged 6 months (c') and aged 1 year (c''); sample D fresh (d) and aged one year (d').

using Gaussian–Lorentzian curves in order to determine the binding energy of the different element core levels more accurately. The Co 2p core level signal was measured with non-monochromatic Al K $\alpha$  radiation because interferences from the oxygen KVV Auger occur in the Co 2p region by using Mg K $\alpha$  radiation

### 2.3. Catalytic measurements

The catalytic experiments were carried out in a flow fixed-bed tubular silica glass reactor. The Gas Hourly Space Velocity (GHSV)

effect was investigated by loading different amount of catalysts; in the former case 44.1 mg of catalyst were mixed with 440 mg of silica glass particles (60–70 mesh sieved) while in the latter 7.4 mg of catalyst were mixed with 476.7 mg of silica glass, in order to maintain the same reactor volume. The fed gas had the following composition: 8.3% ethanol, 50.1% H<sub>2</sub>O and 41.6% helium, giving rise to GHSV values of 51,700 h<sup>-1</sup> and 324,000 h<sup>-1</sup> calculated on the catalyst volume. The reaction temperature was varied as follows: 523 K → 573 K → 673 K → 773 K → 673 K → 573 K → 523 K, with the reaction held at each temperature for 1 h. Repeatability was tested

**Table 1**ESR on sample A: fresh catalyst tested at 51,700 h<sup>-1</sup>(a) and 324,000 h<sup>-1</sup> (b) and aged catalyst tested at 51,700 h<sup>-1</sup>(c) and 324,000 h<sup>-1</sup>(d).

a: ESR GHSV 51,700 h <sup>-1</sup> (fresh)														
T [K]	X C <sub>2</sub> H <sub>6</sub> O	X H <sub>2</sub> O	Y H <sub>2</sub>	S CH <sub>4</sub>	S CO	S CO <sub>2</sub>	S CH <sub>2</sub> CH <sub>2</sub>	S CH <sub>3</sub> CH <sub>3</sub>	S CH <sub>3</sub> CHO	S CH <sub>3</sub> COCH <sub>3</sub>	S C <sub>4</sub> H <sub>8</sub> O <sub>2</sub>	S CH <sub>3</sub> COOH		
523	0.01	0.00	0.00	0.00	0.00	0.00	0.01	0.00	0.64	0.00	0.35	0.00		
573	0.49	0.01	0.09	0.01	0.04	0.02	0.00	0.00	0.90	0.00	0.01	0.01		
673	0.98	0.12	0.35	0.05	0.18	0.18	0.02	0.01	0.21	0.01	0.22	0.12		
773	1.00	0.37	0.82	0.06	0.21	0.70	0.00	0.03	0.00	0.00	0.00	0.00		
673	1.00	0.31	0.69	0.13	0.12	0.65	0.02	0.03	0.01	0.04	0.00	0.00		
573	0.55	0.02	0.13	0.03	0.05	0.08	0.00	0.01	0.70	0.01	0.13	0.00		
523	0.22	0.00	0.04	0.00	0.01	0.03	0.00	0.00	0.73	0.17	0.07	0.00		
b: ESR GHSV 324,000 h <sup>-1</sup> (fresh)														
T [K]	X C <sub>2</sub> H <sub>6</sub> O	X H <sub>2</sub> O	Y H <sub>2</sub>	S CH <sub>4</sub>	S CO	S CO <sub>2</sub>	S CH <sub>2</sub> CH <sub>2</sub>	S CH <sub>3</sub> CH <sub>3</sub>	S CH <sub>3</sub> CHO	S C <sub>4</sub> H <sub>8</sub> O <sub>2</sub>				
523	0.00	0.00	0.00	0.00	0.00	0.00	0.00	1.00	0.00					
573	0.14	0.00	0.02	0.00	0.00	0.01	0.00	0.99	0.00					
673	0.72	0.05	0.22	0.07	0.15	0.12	0.01	0.61	0.03					
773	0.98	0.40	0.83	0.04	0.06	0.80	0.01	0.08	0.00					
673	0.37	0.06	0.16	0.04	0.04	0.33	0.03	0.51	0.06					
573	0.09	0.00	0.02	0.00	0.00	0.08	0.00	0.92	0.00					
523	0.01	0.00	0.00	0.00	0.00	0.00	0.00	1.00	0.00					
c: ESR GHSV 51,700 h <sup>-1</sup> (after 15 days)														
T [K]	X C <sub>2</sub> H <sub>6</sub> O	X H <sub>2</sub> O	Y H <sub>2</sub>	S CH <sub>4</sub>	S CO	S CO <sub>2</sub>	S CH <sub>2</sub> CH <sub>2</sub>	S CH <sub>3</sub> CH <sub>3</sub>	S CH <sub>3</sub> CHO	S CH <sub>3</sub> COCH <sub>3</sub>	S C <sub>4</sub> H <sub>8</sub> O <sub>2</sub>			
523	0.02	0.00	0.00	0.00	0.00	0.00	0.00	0.00	1.00	0.00	0.00			
573	0.42	0.01	0.08	0.02	0.04	0.02	0.00	0.00	0.89	0.00	0.02			
673	1.00	0.31	0.66	0.22	0.10	0.67	0.00	0.01	0.00	0.00	0.00			
773	1.00	0.33	0.71	0.16	0.17	0.65	0.00	0.01	0.00	0.00	0.00			
673	1.00	0.30	0.66	0.16	0.14	0.62	0.02	0.01	0.04	0.01	0.00			
573	0.36	0.02	0.09	0.02	0.02	0.09	0.00	0.00	0.84	0.01	0.02			
523	0.10	0.00	0.02	0.00	0.00	0.02	0.00	0.00	0.98	0.00	0.00			
d: ESR GHSV 324,000 h <sup>-1</sup> (after 15 days)														
T [K]	X C <sub>2</sub> H <sub>6</sub> O	X H <sub>2</sub> O	Y H <sub>2</sub>	S CH <sub>4</sub>	S CO	S CO <sub>2</sub>	S CH <sub>2</sub> CH <sub>2</sub>	S CH <sub>3</sub> CH <sub>3</sub>	S CH <sub>3</sub> CHO	S CH <sub>3</sub> COCH <sub>3</sub>	S DEE			
523	0.02	0.00	0.00	0.00	0.00	0.00	0.00	0.00	0.77	0.23	0.00			
573	0.08	0.02	0.06	0.08	0.33	0.51	0.02	0.00	0.00	0.07	0.00			
673	0.88	0.24	0.58	0.15	0.31	0.51	0.02	0.01	0.00	0.01	0.00			
773	1.00	0.34	0.73	0.15	0.16	0.68	0.00	0.01	0.00	0.00	0.00			
673	0.48	0.05	0.17	0.03	0.05	0.21	0.04	0.00	0.65	0.01	0.01			
573	0.24	0.00	0.05	0.01	0.02	0.04	0.02	0.00	0.89	0.01	0.02			
523	0.03	0.00	0.00	0.00	0.00	0.00	0.00	0.00	0.66	0.16	0.18			

by repeating several experiments. Typical obtained data are given in the Tables.

Product analysis was performed with a gas-chromatograph Agilent 4890 equipped with a Varian capillary column "Molsieve 5A/Porabond Q Tandem" and TCD and FID detectors in series. Between them a nickel catalyst tube was employed to reduce CO<sub>x</sub> to CH<sub>4</sub>. Products analysis was also performed on GC/MS (FOCUS and ISQ from Thermo-Fisher), in order to have a precise identification of the compounds. The conversion of the reactants is defined as follows:

$$X_{\text{reactant}} = \frac{n_{\text{react.in}} - n_{\text{react.out}}}{n_{\text{react.in}}} \quad (1)$$

while selectivity to C-product *i* is defined as:

$$S_i = \frac{n_i}{v_i(n_{\text{react.in}} - n_{\text{react.out}})} \quad (2)$$

where *n<sub>i</sub>* is the number of moles of compound *i*, and *v<sub>i</sub>* is the ratio of stoichiometric reaction coefficients. The hydrogen yield is defined as:

$$Y_{\text{H}_2} = \frac{n_{\text{H}_2\text{out}}}{6 * (n_{\text{ethanol.in}})} \quad (3)$$

### 3. Results and discussion

#### 3.1. Separation, behavior and characterization of catalyst A

Catalyst A was prepared as indicated in the experimental section. In this case, the separation of the nanopowder from the reacting medium was performed by magnetic decantation, as well as the subsequent washings with deionized water and air drying.

The freshly prepared catalyst A does not show any crystalline phase from XRD analysis (Fig. 1a), but after annealing at 773 K it shows the peaks of cobalt boride, Co<sub>2</sub>B, with those of cubic Co (Fig. 1b). The FE-SEM image of the fresh sample (Fig. 2a) shows very small metal particles with an average diameter of about 30 nm. The IR spectrum of the powder is reported in Fig. 3a. It is essentially flat, and does not show bands of significant intensities. This excludes the presence of significant amounts of insulating amorphous phases which give rise to an IR spectrum, such as oxides and borates.

In Table 1a the results of catalytic ESR experiments over catalyst A are reported. This experiment has been performed two days after the preparation of the sample using 44.1 mg of catalyst, and with a GHSV of 51,700 h<sup>-1</sup>. These are exactly the same conditions of the experiment reported in our previous publication [23]. The ethanol conversion is essentially zero at 523 K, but it is relevant at 573 K and essentially complete at 673 K and 773 K. However, only at 773 K steam reforming is complete, with a small coproduction of methane, and a very high hydrogen yield (82%). As reported previ-

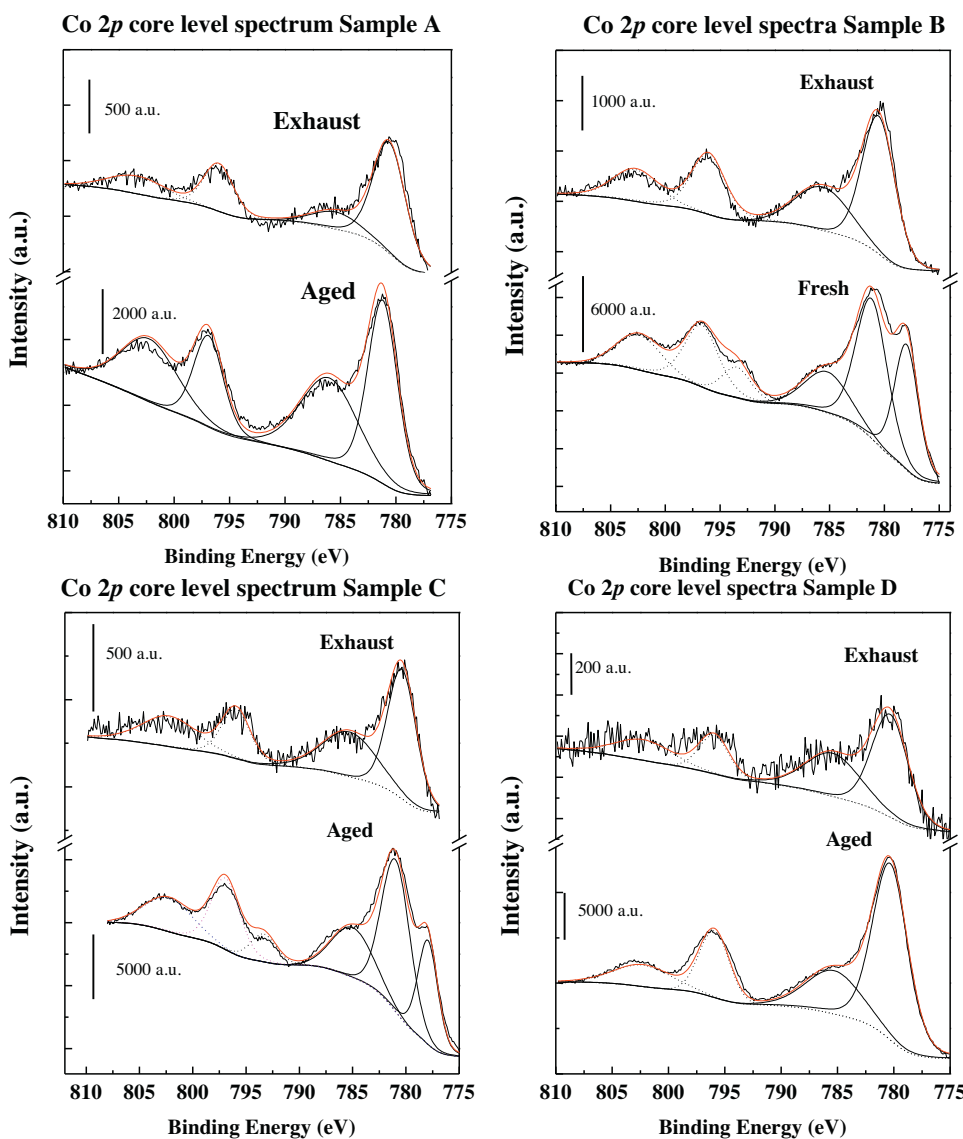


**Fig. 4.** Co 2p XPS core level spectra of fresh or aged and exhaust catalysts.

ously [23], under these conditions the thermodynamic equilibrium for the steam reforming reaction to  $\text{CO} + \text{CO}_2 + \text{H}_2$  is nearly reached, while the methane formation is null.

At lower temperature, the catalyst produces acetaldehyde by dehydrogenation reaction. In the decreasing temperature experiment, at 673 K the catalyst retains high steam reforming activity, showing that in some way it becomes “conditioned”. However, methane production increases thus the hydrogen yield is lower. The results obtained are indeed similar to those reported previously [23], showing a good reproducibility of the preparation method as well as of the catalytic experiment set up.

The same catalyst was also tested using 7.4 mg of catalyst in the bed, with the same feed (Table 1b). Thus, in this case the GHSV is much higher, near  $324,000 \text{ h}^{-1}$ . As expected, ethanol conversion is lower than in the previous experiment at 573 and 673 K, due to the effect of the reduced contact time. However, at 773 K the conversion is complete also under these conditions, with the same hydrogen yield (83%), being steam reforming the largely predominant reaction with small amounts of methane as the only coproduct. In these conditions the product composition is the same irrespective of space velocity, showing that also at the highest space velocity the equilibrium for steam reforming is reached at 773 K. Thus the

catalytic activity for these Co NPs is even higher than that observed before. The methane yield is even lower at high space velocity (SV) than at lower SV, and well below than that expected by thermodynamics, showing that methane formation is strongly kinetically hindered over this catalyst, at 773 K.

When the reaction temperature is lowered back to 673 K at  $324,000 \text{ h}^{-1}$ , conversion is strongly reduced and the steam reforming activity is almost vanished and the main product is acetaldehyde. At the same temperature but lower SV, instead, SR activity was still relevant. This supports the idea that acetaldehyde is an intermediate in steam reforming of ethanol, being formed only at higher space velocity. Methane yield is still low.

The same catalyst A was tested fifteen days after the first catalytic test (Table 1c and d). In the meantime, the powder was conserved in air (aged sample). In the experiment performed at  $51,700 \text{ h}^{-1}$  (Table 1c) the catalyst behavior, although generally comparable with the previous experiment at the same GHSV, was remarkably worsened, with a maximum hydrogen yield of 71% at 773 K, essentially due to an higher production of methane (16%). The data suggest that again at 773 K the steam reforming reaction approaches equilibrium. However, additionally, the production of methane on the “aged” catalyst is more relevant than that observed

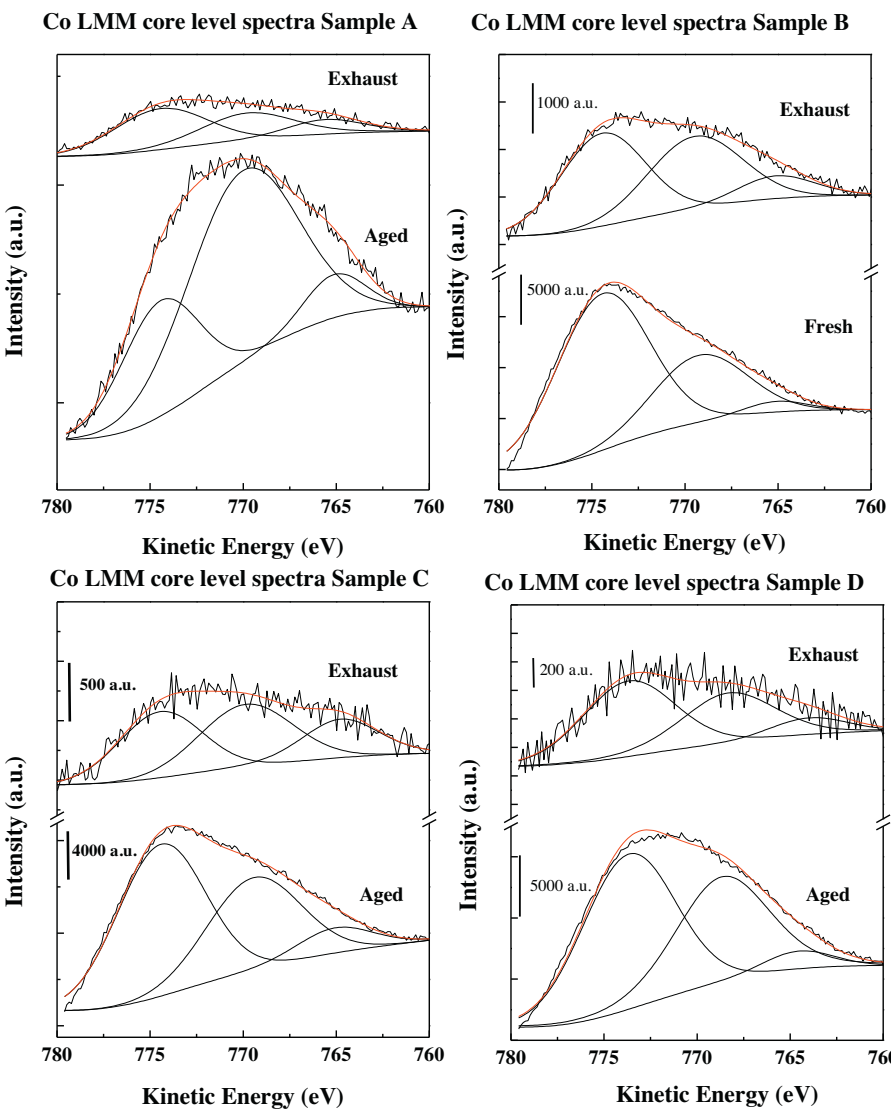


**Fig. 5.** Co LMM Auger spectra of fresh, aged and exhaust catalysts.

on the fresh one, although still kinetically hindered. Thus, the aged catalyst is no more fully selective for ESR at 773 K, producing also significant amounts of methane, likely through ethanol decomposition pathway (CO and methane selectivity are equal).

Also the experiment at GHSV 324,000 h<sup>-1</sup> (Table 1d) has been repeated on catalyst A after aging, it confirms that the catalytic activity is worsened, although only partially. Again, hydrogen yield at 773 K is reduced by an increased production of methane. Also the aged catalyst at 673 K and high SV is more likely a dehydrogenation catalyst, giving rise to acetaldehyde with high yields, than a steam reforming catalyst.

To try an interpretation of the phenomenon of ageing, we repeated characterization experiments with the aged catalyst. The aged sample shows no more a complex XRD pattern (Fig. 1c), but a simpler one, where the strongest peaks are those of the boride phase Co<sub>2</sub>B, together with the peaks of cubic Co metal. The IR spectrum (Fig. 3a') is also significantly modified upon ageing, showing now quite intense bands at 1346 and 1016 cm<sup>-1</sup>, which can be attributed to B=O stretching modes of trigonal and tetrahedral borate species, respectively.

Investigation of the chemical state of each element was carried out by using XPS. The Co 2p XPS spectrum of the same catalyst, aged one year, is reported in Fig. 4A. The spectrum shows the doublet Co

2p<sub>3/2</sub> (solid) and Co 2p<sub>1/2</sub> (dotted). If the Co 2p<sub>3/2</sub> component is considered, two contributions are noticeable. The main Co 2p<sub>3/2</sub> peak appears at 781.0 eV that could be associated to Co<sup>2+</sup>/Co<sup>3+</sup> species accompanied with the typical shake-up satellite with a separation of 4.8 eV that assesses the presence of Co<sup>2+</sup> ions. The XPS spectrum does not show in this case the peak of zero-valent cobalt, found usually in the case of the spectra of the fresh samples (not recorded in this case) near 778 eV [26]. The CoLMN Auger signal is more sensitive to chemical state modifications of cobalt and for this reason in order to better understand the chemical state of Co species present the CoLMN Auger signal was also analyzed. The corresponding spectra in terms of kinetic energy (KE) of CoLMN electrons are depicted on Fig. 5. Three peaks are observed at about 774, 768 and 765 eV indicating the presence of three main ion species of cobalt. The signal at about 768 eV is the main one. In order to perform a tentative assignment of these components the corresponding modified Auger parameter ( $\alpha'$ ) was determined according to the following equation:

$$\alpha' = 1486.6 + \text{KE}_{\text{CoLMN}} - \text{KE}_{\text{Co}2p} \quad (4)$$

where KE (CoLMN) is the kinetic energy of the CoLMN Auger electron, KE Co 2p is the kinetic energy of the Co 2p<sub>3/2</sub> photo-electron and 1486.6 is the energy of the Al K $\alpha$  X-ray excitation

**Table 2**

Binding Energy and modified Auger parameters of Cobalt based catalysts aged (a), fresh (f) and used (u).

Sample		BE Co 2p <sub>3/2</sub> (eV)		$\alpha'$ (eV)		
		Co <sup>0</sup>	Co <sup>2+</sup> /Co <sup>3+</sup>			
A	a	—	781.2	1555.6	1551.3	1546.3
	u	—	780.6	1555.0	1550.4	1546.2
B	f	777.9	781.2	1555.6	1550.4	1546.3
	u	—	780.5	1554.9	1550.0	1545.6
C	a	778.0	781.1	1555.8	1550.5	1546.1
	u	—	780.4	1554.8	1550.2	1545.2
D	a	—	780.3	1554.0	1548.9	1544.9
	u	—	780.3	1554.0	1548.6	1544.3

**Table 3**

Atomic concentration of aged (a) or fresh (f) and used (u) cobalt catalysts determined by XPS.

Sample	C 1s	O 1s	Co 2p	Cl 2p	Na 1s	B 1s
A	a	58.52	26.71	4.87	2.10	1.60
	u	91.78	7.30	0.92	0.00	0.00
B	f	17.24	46.57	19.77	0.40	0.81
	u	90.66	7.60	1.75	0.00	0.00
C	a	26.04	45.39	15.21	0.29	0.00
	u	89.01	10.29	0.70	0.00	0.00
D	a	20.14	49.68	18.84	0.29	0.58
	u	90.51	8.88	0.61	0.00	0.00

source in eV. All these parameters are included in **Table 2**. Three sets of points can be observed; one in the Co<sup>2+</sup> region (CoO or Co(OH)<sub>2</sub>) ( $\alpha' = 1551.3\text{--}1548.6\text{ eV}$ ), another one in the Co<sup>3+</sup> region ( $\alpha' = 1555.6\text{--}1554.0\text{ eV}$ ) [27] and a third one at  $\alpha' = 1544.3\text{--}1546.3\text{ eV}$ . The value at 1546.3 eV could be assigned to Co-B entities, where cobalt is in oxidation state close to zero and there is an electron transfer from Co to B. The fact that XRD pattern clearly shows the presence of Co<sub>2</sub>B and this phase is not clearly observable from XPS, but only as a small contribution in the Auger spectrum is due to the superficial passivation of cobalt particles. It should be kept in mind the superficial nature of XPS technique. Finally, Boron 1s core level spectrum of this sample is represented in **Fig. 6A**. The B 1s core level spectrum shows for this aged sample only a contribution at 191.8 eV assigned to trivalent boron [28].

With regard to the C 1s core level signal, the corresponding spectra are included in **Fig. 7A**. The spectrum of aged A sample presents three contributions: one at 284.8 eV due to adventitious carbon; a second one at about 286.5 eV and characteristic to C–O bonds and the third one close to 289 eV assigned to the presence of surface carbonate [28].

The surface atomic concentration of the studied catalysts is included in **Table 3**. The amount of surface cobalt in sample A is relatively low, 4.87%. The sample shows a great quantity of carbon on the surface, much higher than that observed for the other samples. Moreover, data compiled in **Table 3** indicate that the amount of boron for the aged catalysts is high (13–15%), sample A presents again the lowest value 6.2%; as well as minor quantities of chlorine and sodium.

Catalyst A has also been characterized after use in ESR. XRD pattern still shows the features of cubic cobalt (**Fig. 1c**). IR study was not possible due to the co-presence of silica glass particles after the use in the catalytic bed. The Co 2p core level spectrum of the exhausted sample A presents the same peaks that were observed in the case of the aged samples. The CoLMN core level spectrum decreased in intensity, still presenting the three features attributed to the three Co species, while the Boron 1s core level spectrum is fully vanished. The C 1s core level spectrum shows even four peaks besides those at 284.8 eV (“adventitious carbon” and aliphatic and aromatic carbons, including carbon nanotubes), at 286.5 eV C–O bonds, and

## B 1s core level spectra

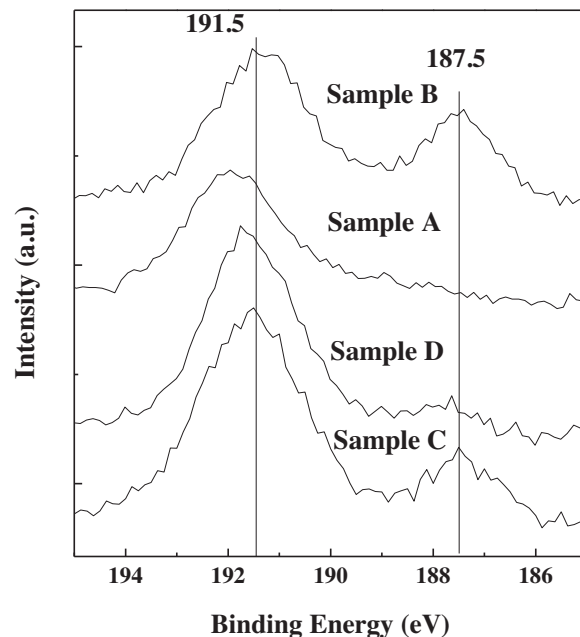


**Fig. 6.** Boron 1s XPS core level spectra of fresh and aged catalysts.

289 eV surface carbonate; a fourth peak is observed near 291.0 eV due to  $\pi \rightarrow \pi^*$  interactions characteristic of aromatic or double bond delocalization. We can mention that, in our previous paper [23], confirmed in this case, FE-SEM study on exhaust Co nanoparticles prepared in the same way, showed significant amounts of carbon nanotubes as a result of catalytic activity (**Fig. 2b**).

### 3.2. Separation, behavior and characterization of sample B

Catalyst B has been prepared by the same procedure as catalyst A, as reported in the experimental section. However, in this case the separation of the nanopowder from the reacting medium has been performed by centrifugation because the particles were too small to be separated by filtration.

The XRD pattern of this sample is again flat but shows after annealing at 773 K the reflection peaks of Co<sub>2</sub>B with small amounts of cubic cobalt (**Fig. 8B**), thus appearing similar to sample A.

The Co 2p core level spectrum of the fresh sample, shows (**Fig. 4B**) one contribution at about 778.0 eV assigned to metallic Co, and a second one, with higher intensity, at 781.1 eV that could be associated to the presence to Co<sup>2+</sup>/Co<sup>3+</sup> ions in accordance with the presence of the broad ill-defined shake-up satellite at about 787.0 eV [27,29]. The Boron 1s core level spectrum (**Fig. 6B**) shows two contributions at 191.5 and 187.5 eV. The first one is assigned to oxidised boron- species (borate species), meanwhile the second one is 0.5 eV higher than the value reported for elemental boron and indicating the presence of an electronic transfer between B–Co.

IR spectrum of the fresh catalyst (**Fig. 3b**) shows the presence of surface borates with two broad features at 1362 cm<sup>-1</sup> and 936 cm<sup>-1</sup>.

Catalytic activity of this sample is reported in **Table 4**. The catalyst is less active than catalyst A. Tested as fresh, it demonstrates activity already at low temperature in ethanol dehydrogenation to acetaldehyde at 523 and 573 K. By temperature increment at 673 K some activity toward steam reforming starts but acetaldehyde remains as the main product. At the maximum reaction temperature ethanol conversion arrived at 78% giving rise to a hydrogen yield of 57% since still acetaldehyde was detected as product. In

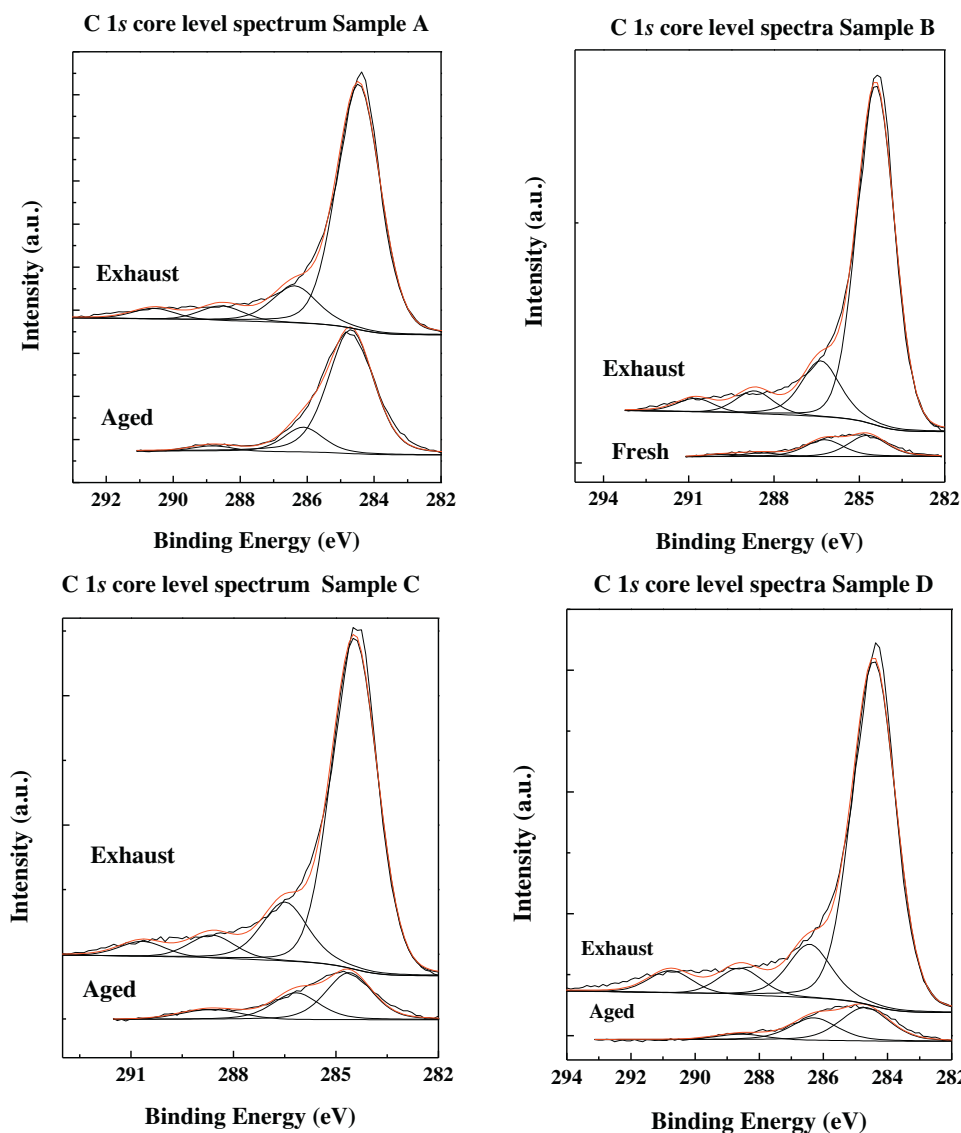


**Fig. 7.** Carbon 1s XPS core level spectra of fresh, aged and exhaust catalysts.

**Table 4**

ESR with a GHSV of  $324,000 \text{ h}^{-1}$  on sample B fresh.

T [K]	X $\text{C}_2\text{H}_6\text{O}$	X $\text{H}_2\text{O}$	Y $\text{H}_2$	S $\text{CH}_4$	S CO	S $\text{CO}_2$	S $\text{C}_2\text{H}_4$	S $\text{CH}_3\text{CHO}$	S $\text{C}_3\text{H}_6\text{O}$
573	0.27	0.00	0.05	0.01	0.02	0.01	0.00	0.95	0.00
623	0.23	0.00	0.04	0.01	0.03	0.01	0.00	0.95	0.00
673	0.65	0.09	0.27	0.04	0.08	0.28	0.00	0.59	0.00
773	0.78	0.25	0.57	0.05	0.12	0.64	0.00	0.19	0.00
673	0.51	0.13	0.30	0.03	0.04	0.51	0.00	0.41	0.01
573	0.12	0.00	0.03	0.00	0.01	0.07	0.00	0.91	0.00
523	0.01	0.00	0.00	0.00	0.00	0.00	0.00	1.00	0.00

the decreasing temperature experiment at 673 K, the catalyst was slightly more selective to steam reforming reaction even if ethanol reached a lower conversion (51%). By further reaction temperature reduction, the conversion falls down producing as main product acetaldehyde.

The catalyst has been characterized after catalysis through XPS technique. In particular the Co 2p core level spectrum of the exhausted sample, no more shows the component of zero-valent cobalt but only those related to oxidized cobalt at 780.5 eV. Also in this case the Boron 1s spectrum vanished after catalytic experiment while four components are again observed in the Carbon 1s core

level spectrum, likely due to the formation of nanotubes (Fig. 7B), as already shown for A sample in Fig. 2b.

### 3.3. Separation, behavior and characterization of sample C

Catalyst C has been prepared and separated by the same procedure as catalyst A, however, in this case the sample has been dried in air, not under vacuum in order to increase the cobalt phase instead of  $\text{Co}_2\text{B}$ , according to reference [24].

The XRD pattern of this sample is again flat but shows the peaks of cubic Co with small amounts of the boride  $\text{Co}_2\text{B}$  after annealing

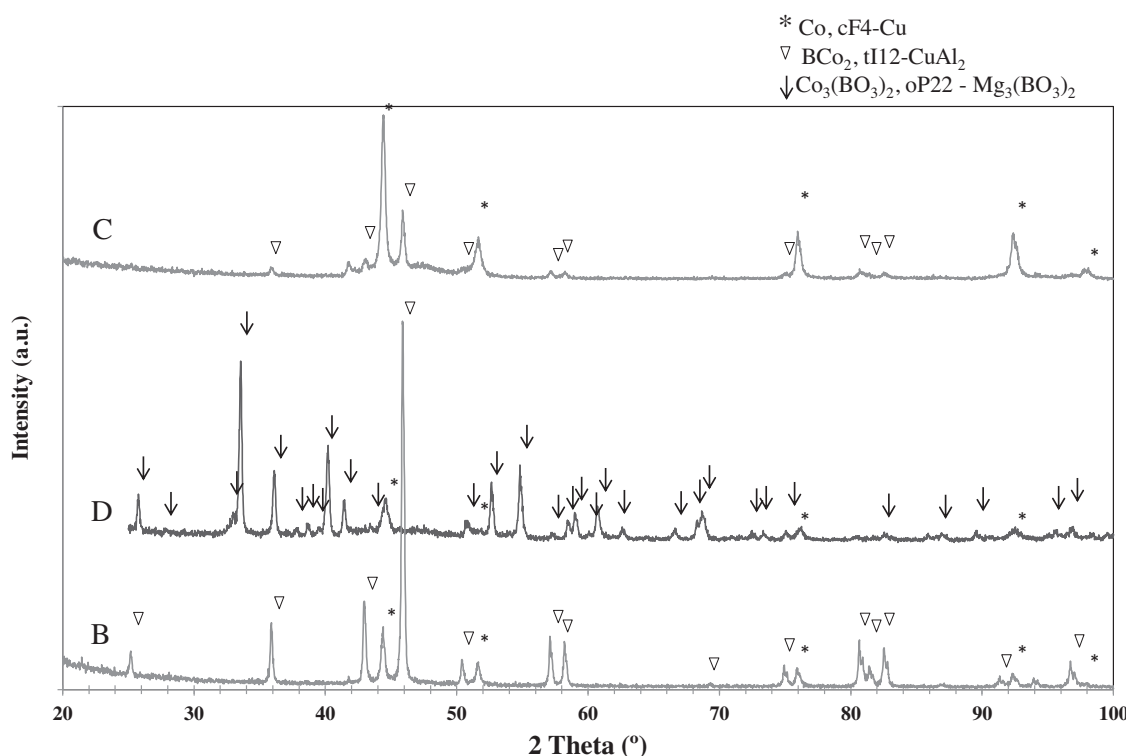


**Fig. 8.** XRD of B–D catalysts after annealing at 773 K for 3 h in Ar.

at 773 K (Fig. 8C), thus showing the same phases revealed already for sample A. However, the IR spectrum (Fig. 3c) shows bands at 1400 cm<sup>-1</sup> and 971 cm<sup>-1</sup> markedly intense, showing the presence of trigonal and tetrahedral borate species.

This sample was tested at 773 K and 324,000 h<sup>-1</sup> as a function of the time on stream (TOS) in order to evaluate the performances and the stability at the highest reaction temperature, where sample A was showing its best performances even at 324,000 h<sup>-1</sup>. The results are reported in Fig. 9 as a function of time on stream. The catalyst maintained almost constant its performances during all the catalytic test with an average hydrogen yield of 76% since the coproduction of methane from catalytic ethanol decomposition may be due to the presence of surface borate. It should be mentioned that during the test a pressure drop of 0.3 bar was reached due to coking of the catalyst that was not affecting the catalytic activity drastically.

The catalyst has been aged for six months and after this, catalytic activity and IR were performed in order to detect the sample behavior. After one year the characterization was repeated. The catalytic activity performed on the six months aged sample at 324,000 h<sup>-1</sup> GHSV results definitely worse than the fresh performance and that of sample A even after ageing 15 days (Table 5). At 773 K, the conversion of ethanol is not complete (78%) and, accordingly, hydrogen yield definitely lower (59%). Additionally, at 673 K both in the increasing reaction temperature experiment and in the decreasing one, the catalyst is most selective for dehydrogenation of ethanol to acetaldehyde, more than for steam reforming.

The IR spectra of the six months aged sample (Fig. 3c') shows a further increase of the band at about 1402 cm<sup>-1</sup> and 870 cm<sup>-1</sup> due to borates species with a possible increase also of bands due to cobalt oxides (700–500 cm<sup>-1</sup>).

After one year, the IR spectrum (Fig. 3c'') shows a further increase of the intensity of the bands due to borates (1393 cm<sup>-1</sup> and 970 cm<sup>-1</sup>) and slightly more evident those related to the cobalt oxide features (700–500 cm<sup>-1</sup>). One the same sample the XPS

shows the presence of zero-valent cobalt both in the Co 2p core level region (see Fig. 4c) together with oxidized cobalt. In the B 1s core level region both borate and boride species were detected while three carbon species are detected in the C 1s core level spectrum, as explained before for other samples.

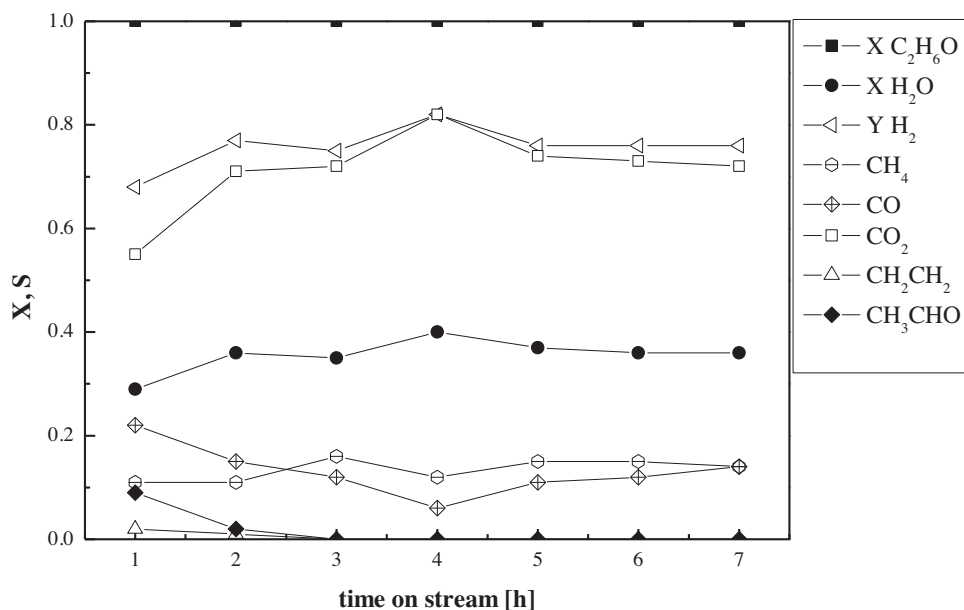
The sample after catalysis followed by 7 month ageing in room atmosphere, no more shows in the Co 2p core level region the peak of zero-valent cobalt (see Fig. 4C) but the CoLMM spectra show it (see Fig. 5C). Also in this case, the boron signal vanished and the intensity of the Carbon 1s signal (Fig. 7C) grows very much evidencing one new component due to carbon nanotubes signal. Again, the surface composition shows greater quantities of Co and boron, than for A samples; but higher carbon content than for B catalyst. After testing, C is the main element present on the surface

### 3.4. Separation, behavior and characterization of sample D

Catalyst D has been prepared by the same procedure but, in this case, the separation of the nanopowder from the reacting medium has been performed by filtration on a glass frit, washed on the filter with 300 ml of deionized water and dried in air, in order to maximise boron species oxidation.

The XRD pattern of this sample after annealed at 773 K shows the reflection lines of the borate phase Co<sub>3</sub>B<sub>2</sub>O<sub>6</sub>, together with those of cubic Co (Fig. 8D). Accordingly, the IR spectrum shows bands at 1383 and 982 cm<sup>-1</sup> markedly intense, showing the presence of both trigonal and tetrahedral borate species in a significant amount. The spectrum also shows (see Fig. 3d) the additional typical features of the Co<sub>3</sub>O<sub>4</sub> spinel at 664 and 594 cm<sup>-1</sup>. The XPS spectrum (Fig. 4D), recorded on the aged sample, does not show the spectrum of zero-valent cobalt and very weak that of boride species. The CoLMM spectrum is similar than those observed for other samples, with the coexistence of Co<sup>2+</sup>–Co<sup>3+</sup> and also Co–B species.

The catalytic performance at 324,000 h<sup>-1</sup> GHSV for this sample is definitely worse than that observed for sample A but better

**Fig. 9.** ESR time on stream for C sample at 324,000 h⁻¹.**Table 5**

ESR with a GHSV of 324,000 h⁻¹ on sample C aged six months.

T (K)	X C <sub>2</sub> H <sub>6</sub> O	X H <sub>2</sub> O	Y H <sub>2</sub>	S CH <sub>4</sub>	S CO	S CO <sub>2</sub>	S CH <sub>3</sub> CHO	S C <sub>4</sub> H <sub>8</sub> O <sub>2</sub>	S CH <sub>3</sub> COOH
523	0.00	0.00	0.00	0.00	0.00	0.00	0.00	0.00	0.00
573	0.34	0.00	0.07	0.02	0.04	0.02	0.93	0.00	0.00
673	0.72	0.07	0.23	0.07	0.14	0.13	0.56	0.00	0.10
773	0.78	0.27	0.59	0.10	0.14	0.69	0.07	0.00	0.00
673	0.35	0.07	0.17	0.04	0.05	0.37	0.51	0.03	0.00
573	0.08	0.00	0.02	0.00	0.00	0.06	0.94	0.00	0.00
523	0.01	0.00	0.00	0.00	0.00	0.00	1.00	0.00	0.00

**Table 6**

ESR with a GHSV of 324,000 h⁻¹ on sample D fresh.

T (K)	X C <sub>2</sub> H <sub>6</sub> O	X H <sub>2</sub> O	Y H <sub>2</sub>	S CH <sub>4</sub>	S CO	S CO <sub>2</sub>	S CH <sub>2</sub> CH <sub>2</sub>	S CH <sub>3</sub> CHO	S C <sub>4</sub> H <sub>8</sub> O <sub>2</sub>	S CH <sub>3</sub> COOH
523	0.01	0.00	0.00	0.00	0.00	0.00	0.00	1.00	0.00	0.00
573	0.15	0.00	0.03	0.00	0.00	0.00	0.00	1.00	0.00	0.00
673	0.60	0.04	0.17	0.05	0.10	0.07	0.01	0.58	0.01	0.18
773	0.86	0.31	0.67	0.11	0.15	0.71	0.02	0.02	0.00	0.00
673	0.29	0.06	0.15	0.04	0.03	0.45	0.02	0.46	0.00	0.00
573	0.08	0.00	0.02	0.00	0.00	0.08	0.00	0.92	0.00	0.00
523	0.01	0.00	0.00	0.00	0.00	0.00	0.00	1.00	0.00	0.00

than for samples B and C (**Table 6**). At 773 K the conversion is not complete (86%) and hydrogen yield is 67%. Additionally, at 673 K both in the increasing reaction temperature experiment and in the decreasing one, the catalyst is most selective for dehydrogenation of ethanol to acetaldehyde, more than for steam reforming.

The Co 2p spectrum (see Fig. 4D) of the exhaust sample is close to the aged sample but with lower intensity. The CoLMM spectrum is also close to the aged sample. Also in this case the B 1s signal vanished and the intensity of the C 1s signal grows very much (Fig. 7D) evidencing one new component due to the formation carbon nanotubes.

#### 4. Conclusions

The main conclusions of the present study may be summarized as follows:

Metallic nanoparticles prepared by reduction of cobalt chloride by sodium boro hydride are active catalysts for ethanol steam

reforming at moderate temperature. In particular, they give rise to nearly full ethanol conversion and hydrogen yields of the order of 83% when tested at 773 K, GHSV 324,000 h⁻¹ with diluted 1:6 ethanol: water feed in He 41.6%. The amount of coproduced methane is very low (yield <0.05). The best catalytic materials have a stable activity at 773 K for 8 h although the formation of carbonaceous materials is evident with time on stream. Experiments performed at different space velocities provide evidence of the intermediate formation of acetaldehyde in the ethanol steam reforming path.

The catalysts appear amorphous at XRD prior to use and contain, according to XPS analysis, together with cubic metallic cobalt also boron species (borides and borates) but are also contaminated by sodium, chlorine and carbon species. After annealing, crystalline cubic cobalt and different cobalt borides usually appear. However depending on the preparation method also cobalt borates could be observed. After use in ESR, the surface contamination of Na, Cl and B appear to vanish due either to volatilization or to coverage by carbon species.

The surface properties of these materials are very sensitive to the condition of separation from the reaction medium at the end of the preparation step, and to the conditions of ageing and storage in the laboratory.

An increasing time of ageing seems to favor the formation of borates species and the observed oxidation of metallic cobalt to cobalt oxides. Although a possible role of other minor impurities, such as chlorine and sodium, cannot be excluded at this time, it seems likely that these phenomena can be associated to the loss in the catalytic activity that results in a lower ethanol conversion, lower hydrogen yield and sometimes higher selectivity to acetaldehyde.

## Acknowledgements

The collaboration with Lea Pasquale on the frame of her master thesis is acknowledged. Project of Excelencia P12 RNM 1565 funded by Junta de Andalucía and FEDER funds are also acknowledged.

## References

- [1] A. Haryanto, S. Fernando, N. Murali, S. Adhikari, *Energy Fuels* 19 (2005) 2098–2106.
- [2] D. Vaidya, A.E. Rodrigues, *Chem. Eng. J.* 117 (2006) 39–49.
- [3] M. Ni, D.Y.C. Leung, M.K.H. Leung, *Int. J. Hydrogen Energy* 32 (2007) 3238–3247.
- [4] F. Frusteri, S. Freni, *J. Power Sources* 173 (2007) 200–209.
- [5] P. Ramirez de la Piscina, N. Homs, *Chem. Soc. Rev.* 37 (2008) 2459–2467.
- [6] A. Bshish, Z. Yaako, B. Narayanan, R. Ramakrishnan, A. Ebhish, *Chem. Pap.* 65 (2011) 251–266.
- [7] G. Nahar, V. Dupont, *Biofuels* 3 (2012) 167–191.
- [8] N. Bion, D. Duprez, F. Epron, *ChemSusChem* 5 (2012) 76–84.
- [9] L.V. Mattos, G. Jacobs, B.H. Davis, F.B. Noronha, *Chem. Rev.* 112 (2012) 4094–4123.
- [10] C. Burda, X. Chen, R. Narayanan, M.E. El-Sayed, *Chem. Rev.* 105 (2005) 1025–1102.
- [11] S. Alayoglu, C. Aliaga, C. Sprung, G.A. Samorjai, *Catal. Lett.* 141 (2011) 914–924.
- [12] B.C. Ranu, K. Chattopadhyay, L. Adak, A. Saha, S. Bhadra, R. Dey, D. Saha, *Pure Appl. Chem.* 81 (2009) 2337–2354.
- [13] A.Y. Khodakov, W. Chu, P. Fongarland, *Chem. Rev.* 107 (2007) 1692–1744.
- [14] G. Busca, *Heterogeneous Catalytic Materials*, Elsevier, Amsterdam, 2014.
- [15] T.L. Renken, M.W. Forkner, US Patent Application 20080227632 (2008) to Huntsman petr. Co.
- [16] B. Chen, U. Dingderissen, J.G.E. Krauter, H.G.J. Lansink Rotgerink, K. Möbus, D.J. Ostgard, P. Panster, T.H. Riermeier, S. Seebald, T. Tacke, H. Trauthwein, *Appl. Catal.* 280 (2005) 17–46.
- [17] P.R. Likhari, R. Arundhathi, M.L. Kantam, P.S. Prathima, *Eur. J. Org. Chem.* 31 (2009) 5383–5389.
- [18] B.H. Davis, *Greener Fischer-Tropsch Processes for Fuels and Feedstocks*, in: P.M. Maitlis, A. de Klerk (Eds.), Wiley, New York, 2011, pp. 193–200.
- [19] The catalyst technical handbook, Johnson Matthey, 2008, available on internet.
- [20] V.A. de la Peña O'shea, N. Homs, E.B. Pereira, R. Nafria, P. Ramirez de la Piscina, *Catal. Today* 126 (2007) 148–152.
- [21] S. Tutti, F. Pepe, *Catal. Lett.* 122 (2008) 196–203.
- [22] W. Gac, W. Zawadzki, B. Tomaszewska, *Catal. Today* 176 (2011) 97–102.
- [23] G. Garbarino, P. Riani, M.A. Lucchini, F. Canepa, S. Kawale, G. Busca, *Int. J. Hydrogen Energy* 38 (2013) 82–91.
- [24] G.N. Glavee, K.J. Klabunde, C.M. Sorensen, G.C. Hadjipanayis, *Langmuir* 9 (1993) 162–169.
- [25] Pearson Crystal Data: Crystal structure database for inorganic compounds, Release 2009/2012, ASM international, the Material Information Society.
- [26] J. Dillard, C.V. Schenck, M.H. Koppelman, *Clays Clay Miner.* 31 (1983) 69–72.
- [27] A. Infantes-Molina, J. Mérida-Robles, E. Rodríguez-Castellón, B. Pawelec, J.L.G. Fierro, A. Jiménez-López, *Appl. Catal. A* 286 (2005) 239–248.
- [28] J.F. Moulder, W.F. Stickle, P.E. Sobol, K. Bomben, *Handbook of X-ray Photoelectron Spectroscopy*, in: J. Chastain (Ed.), 2nd ed., Perkin-Elmer Corporation (Physical Electronics), 1992.
- [29] S. Gupta, N. Patel, A. Miotello, D.C. Kothari, *J. Power Sources* 279 (2015) 620–625.